

# *UBVRI* Hubble Diagrams of Gamma-ray Burst Supernovae

Zach Cano<sup>1\*</sup> & Páll Jakobsson<sup>1</sup>

<sup>1</sup>*Centre for Astrophysics and Cosmology, Science Institute, University of Iceland, Dunhagi 5, 107 Reykjavik, Iceland.*

Accepted xx. Received xx; in original form xx

## ABSTRACT

In this paper we demonstrate, in principle, how gamma-ray burst supernovae (GRB-SNe) can be used to measure the Hubble constant,  $H_0$ . Using two statistical data-fitting procedures, a linear-least squares (LLS) method and a Monte-Carlo (MC) method, we first present a statistically significant luminosity–decline relationship of GRB-SNe in filters *UBVRI*, and then provide constraints on  $H_0$ . Using SN 1998bw, and a fiducial distance to its host galaxy of 37 Mpc, we constrain  $H_0$  to the range 61–69 km s<sup>−1</sup> Mpc<sup>−1</sup>. In our analysis, we adopt conservative errors of 20% in the SN magnitudes. The subsequent errors in  $H_0$  derived from the MC method are of order 2–4 km s<sup>−1</sup> Mpc<sup>−1</sup>, and roughly ten times larger using the LLS method. Interestingly, the weakest luminosity–decline relation is seen in the *B*-band; however the *B*-band (and *V*-band) data provide one of the tightest constraints on  $H_0$  of all the filters. Finally, as GRB-SNe arise from massive star progenitors, whose lifetimes are of order several million years, they are likely to occur at earlier times in the universe than SNe Ia, as the latter require at least one white-dwarf star in a binary system, which forms only after a few billion years. This suggests that with suitable instrumentation and facilities, GRB-SNe can be found at larger redshifts/earlier times in the universe than SNe Ia, and eventually providing useful constraints on the fundamental cosmological parameters in the early universe.

**Key words:** Keywords

## 1 INTRODUCTION

It was recently shown by Cano (2014; C14 here after) and Li & Hjorth (2014) that gamma-ray burst supernovae (GRB-SNe) have the potential to be used as standardizable candles. In C14, it was shown that a statistically significant correlation was present in the luminosity ( $k$ ) and stretch ( $s$ ) factors of eight GRB-SNe relative to a template SN: SN 1998bw, which was associated with GRB 980425 (e.g. Galama et al. 1998; Patat et al. 2001). In a complementary, but independent analysis, a statistically significant luminosity–decline relationship was seen in the *K*-corrected *V*-band light curves (LCs) of eight GRB-SNe investigated by Li & Hjorth (2014). These results unambiguously demonstrated that GRB-SNe have the potential to be used as standardizable candles.

In the cosmic distance ladder, type Ia SN occupy one of the top-most rungs, helping to determine the distance to objects up to redshifts of almost  $z = 2$  (Jones et al. 2013). Before the luminosity–decline relationship was observed for nine nearby ( $\log(cz) < 4.1$ ) SNe Ia by Phillips (1993), several papers had estimated the Hubble constant

( $H_0$ ) by assuming a single peak luminosity for SNe Ia in a given filter (e.g. Kowal 1968; Sandage & Tammann 1993). The luminosity–decline relationship was used thereafter to calibrate SN data in Hubble diagrams to estimate  $H_0$  (e.g. Hamuy et al., 1995; Perlmutter et al. 1997, who also estimated the mass budget of the universe). The use of SNe Ia as standardizable candles reached a crescendo in the late 1990s and early 2000s, when Riess et al. (1998), Perlmutter et al. (1999) and Freedmann et al. (2001) constrained not only the Hubble constant, but also the mass and energy content of the universe, and demonstrated for the first time the existence of “dark energy”, which is responsible for the accelerated expansion of the cosmos, and makes up almost three-quarters of everything in the universe.

Building upon the preliminary result in C14, in this current paper we demonstrate that GRB-SNe can be used as cosmological probes in much the same fashion as SNe Ia, and provide an estimate of the Hubble constant using our dataset. In Section 2 we outline our method for determining the peak magnitudes and decline rate, given as the  $\Delta m_{15}$  parameter (which is the amount the LC fades from peak light to fifteen days later). In Section 3 we perform two statistical analyses (a linear least squares and a Monte-Carlo

\* zewcano@gmail.com

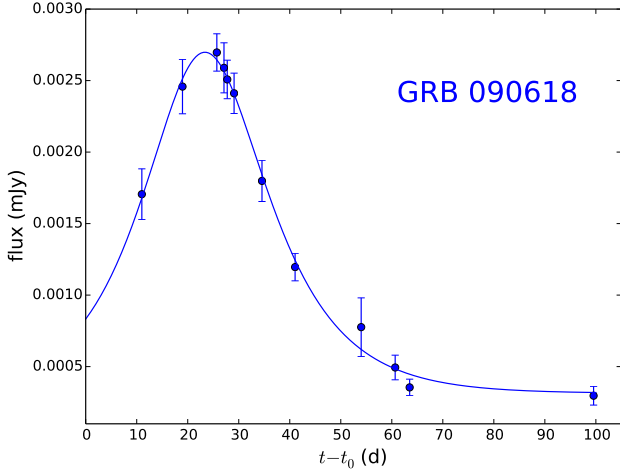


**Figure 1.** An example of fitting the Bazin function (equation 1, shown as solid blue line) to the interpolated  $B$ -band (blue points) LC of GRB 090618 from C14. Note that the parameter  $t_0$  shown on the  $x$ -axis is the trigger time of the GRB, rather than one of the free parameters in the Bazin function.

approach) to (1) look for a luminosity–decline relation in all  $UBVRI$  filters (Section 3.1), and (2) demonstrate how the Hubble constant can be determined, in principle, using GRB-SNe (Section 3.2). In Section 4 we discuss our results and summarize our conclusions.

## 2 METHOD

In this paper, we have returned to the eight GRB-SNe used in the analysis of C14. This time, instead of determining the luminosity and stretch factors relative to a  $K$ -corrected template SN, we have used the SN LCs obtained from his decomposition method. To the isolated SN LCs, we fit a variety of models to determine the (1) peak apparent magnitudes, and (2)  $\Delta m_{15}$  in every interpolated rest-frame filter. The peak absolute magnitudes and  $\Delta m_{15}$  values are presented in Table 1, where we have used a  $\Lambda$ CDM cosmology constrained by Planck (Planck Collaboration et al. 2013) to calculate the former, where  $H_0 = 67.3 \text{ km s}^{-1} \text{ Mpc}^{-1}$ ,  $\Omega_M = 0.315$ ,  $\Omega_\Lambda = 0.685$ . The magnitudes are corrected for observer- and rest-frame extinction, as well as being  $K$ -corrected via spectral energy distribution (SED) interpolation, as discussed in C14.

We fit three different functions to the SN LCs to determine these observational properties: (1) the Bazin function (Bazin et al. 2011; equation 1 in this work), (2) high-order polynomials, and (3) linear splines. All functions were fit to the data using PYTHON scripts. A linear least-squares (LLS) Levenberg-Marquardt algorithm was used via SCIPY.OPTIMIZE to fit the Bazin function to the data, while NUMPY.POLYFIT was used to fit the polynomial to the data. Finally, SCIPY.INTERPOLATE.INTERP1D was used to fit the linear spline to the data.

For most of the GRB-SNe, the LCs were not sampled well enough to use methods (2) and (3), where only the LCs of SN 1998bw were adequately sampled enough to ef-

fectively use these fitting techniques. When fitting the LCs of SN 1998bw with the three different functions, the peak magnitude in each filter did not vary by more than  $0.01^m$ , while the time of peak light varied by no more than 0.15 d.

The remaining GRB-SNe were fitted with the Bazin function:

$$f(t) = \Lambda \left[ \frac{\exp\left(\frac{-(t-t_0)}{\tau_{\text{fall}}}\right)}{1 + \exp\left(\frac{-(t-t_0)}{\tau_{\text{rise}}}\right)} \right] + \Phi \quad (1)$$

The Bazin function is a more elegant empirical model, that possesses fewer free parameters, than the empirical model used in Cano et al. (2011) and Cano (2013) to describe the LC shapes of GRB-SNe and SNe Ibc. It has five free parameters:  $\Lambda$  is a normalization constant,  $\Phi$  an offset constant, and  $\tau_{\text{rise}}$  &  $\tau_{\text{fall}}$  are the rise and fall times of the SN LC.  $t_0$  is related to the rise and fall times, as well as the time of maximum light by  $t_0 = t_{\text{max}} - \tau_{\text{rise}} \times \ln\left(\frac{\tau_{\text{fall}}}{\tau_{\text{rise}} - 1}\right)$ .

Note that we have adopted the conservative 20% error estimated from C14 for the peak magnitudes and  $\Delta m_{15}$  values. This conservative error arises from the fact that the isolation of the SN light involves a complicated decomposition technique (C14), with several sources of error that arise from GRB afterglow modelling and subtraction, the host-galaxy subtraction, the uncertainties in the observer-frame and rest-frame extinction, and the SED interpolation. The 20% error adopted here is much larger than the systematic error associated with the different fitting functions described above.

## 3 ANALYSIS & RESULTS

### 3.1 $M_\nu$ vs. $\Delta m_{15,\nu}$

Figure 2 shows the peak absolute magnitudes of the eight GRB-SNe from C14 versus  $\Delta m_{15}$  in filters  $UBVRI$ . A linear relation was fitted to the data:

$$M_\nu = m \times \Delta m_{15,\nu} + b \quad (2)$$

to determine the slope ( $m$ ) and  $y$ -intercept ( $b$ ). We have used two different approaches to the data fitting: (1) a LLS method using PYXPLOT<sup>1</sup>, and (2) a Monte-Carlo (MC) method using PYTHON.

In approach (1), the LLS fitting is performed using the generic fitting algorithm<sup>2</sup> employed by PYXPLOT, and the fit is “weighted” and performed twice, using first the  $y$ , and secondly the  $x$  errors. We have conservatively adopted the largest errors from each fit. In the MC approach, a new dataset is created from the original by choosing a new value from a Gaussian that is centered on each original datapoint, and whose standard deviation in each direction is equal to the error in that variable. The simulation was performed 10,000 times, each time fitting the straight line to the new

<sup>1</sup> <http://pyxplot.org.uk>

<sup>2</sup> *verbatim* from the PYXPLOT user manual, which can be found on their website.

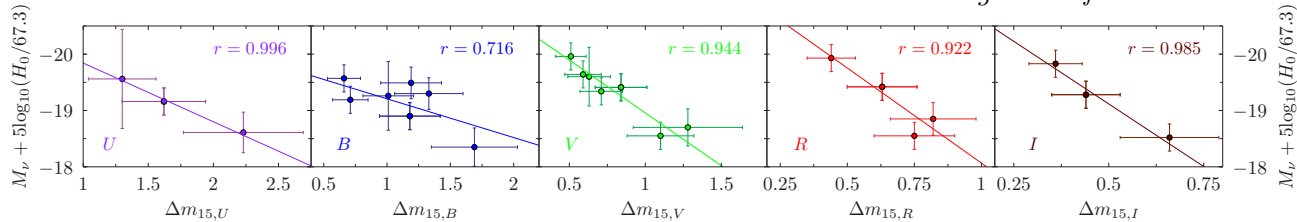


**Figure 2.** Luminosity–decline relations for the eight GRB-SNe from C14 in filters *UBVRI*. The Pearson’s correlation coefficient ( $r$ ) for each filter is shown. It is seen that the relation with the lowest statistical significance is in the *B*-band. However, in Fig. 3, the *B*-band data provides one of the tightest constraint on the Hubble constant of all the filters.

dataset using a non-weighted LLS optimization. The estimated errors of  $m$  and  $b$  arise from their resultant distributions, where the quoted  $1\text{-}\sigma$  errors are the standard deviation of each distribution. Our results are shown in Table 2. On average, the errors from the MC approach are of order to, but slightly larger than, those from the weighted-LLS method.

For each dataset we also calculated the Pearson’s correlation coefficient and the two-point probability of a chance correlation. The largest sample sizes are in *B* and *V* ( $N = 7$ ), while there are only four datapoints in *R*, and three each in *U* and *I*. It is seen, both visually and statistically, that the correlation in the *B*-band is the weakest ( $r = 0.716$ ). Conversely, a strong correlation is seen in the other filters ( $r > 0.92$  for each of the remaining filters), though we must consider the caveat of small sample sizes in *U*, *R* and *I*. A strong correlation is seen in the *V*-band, which supports the statistically significant relation seen in the K-corrected, *V*-band LCs of the GRB-SNe investigated by Li & Hjorth (2014).

We also investigated what the effect of using different values of the input cosmological parameters, namely  $H_0$ , will have on the fitted values of  $m$  and  $b$  in Fig. 2. In each case, the same slope ( $m$ ) was obtained, but with different  $y$ -intercept ( $b$ ) values. For example, when using  $H_0 = 80 \text{ km s}^{-1} \text{ Mpc}^{-1}$  and the LLS method, the *U*-band data had an identical slope ( $m = 1.04 \pm 0.66$ ), but a different intercept ( $b = -20.53 \pm 1.19$ ). This arises from the fact that the peak absolute magnitudes of the three GRB-SNe in the *U*-band are all fainter due to the larger value of  $H_0$  used to calculate the distance modulus. As we will show in the following section, using different values for  $H_0$  in the luminosity–decline relationship has a minimal effect the resultant values of the derived Hubble constant.

### 3.2 The Hubble Constant

Plotted in Fig. 3 are  $\log(cz)$  vs. apparent magnitude of the eight GRB-SNe in filters *UBVRI*. The following equation (e.g. Tammann et al. 2002; Sandage & Tammann 1993) was fitted to the data:

$$\log(cz) = 0.2 \times m_{\text{app}} + \delta \quad (3)$$

to determine the  $y$ -intercept ( $\delta$ ) of the line, which in turn is used to determine  $H_0$  via:

$$\log(H_0) = 0.2 \times M_{\text{abs}} + \delta + 5 \quad (4)$$

The best-fitting values of  $\delta$  are displayed in Table 3.

As in the preceding section, we used both the LLS and MC methods to estimate  $\delta$  and its associated error. It is seen that the errors in  $\delta$  determined via the LLS method are almost ten times larger than those determined via the MC method.

In Fig. 3 we determined  $\delta$  for both the original and “corrected” peak apparent magnitudes, where the corrected magnitudes are determined using the best-fitting values of  $m$  and  $b$  (Table 2), and the value of  $\Delta m_{15}$  for a given GRB-SN in a given filter. Strictly speaking, the correction should be performed using an independent dataset, as noted by Hamuy et al. (1995), who used the independent set of SNe Ia from Phillips (1993) to correct their additional SNe Ia against. However, as we are merely demonstrating the principle and applicability of our method, rather than attempting to precisely determine  $H_0$ , we have corrected our data using the luminosity–decline relation determined with our dataset. Finally, it is seen that the errors in  $\delta$  are much larger for the corrected magnitudes due to the large errors in  $m$  and  $b$  (which are used to calculate the errors in the corrected magnitudes).

To determine the Hubble constant, all one needs to do is use the value of  $\delta$  in a given filter, and the peak absolute magnitude of a GRB-SN whose distance has been independently determined (here we have used SN 1998bw). Our analysis is now limited by the fact that we do not have an independent distance measurement to the host galaxy of SN 1998bw (and thus the “real” absolute magnitudes in *UBVRI*). However, at  $z = 0.00866$  (Li & Hjorth 2014), flat  $\Lambda$ CDM cosmological models that incorporate typical values for the Hubble constant and the mass and energy densities, give distances in the range 36–39 Mpc. For the example here, we have adopted a distance of 37 Mpc, which corresponds to a distance modulus of  $\mu = 32.84 \text{ mag}$ .

Using the “ultimate” LCs from Clacchiati et al. (2011), which are de-reddened and K-corrected, the rest-frame, peak apparent magnitudes of SN 1998bw in filters *UBVRI* are:  $m_U = 13.75$ ,  $m_B = 14.01$ ,  $m_V = 13.50$ ,  $m_R = 13.49$  and  $m_I = 13.63$ . We have determined these by fitting the three functions from Section 3 to the *UBVRI* LCs of SN 1998bw. Each of these is transformed into an absolute magnitude, and plugged into equation 4, along with the corresponding value of  $\delta$  in that filter, to give  $H_0$ . The error in  $H_0$  is determined using the error in  $\delta$ , and the final values in each filter are shown in Table 3.

At this stage, with the small sample sizes and large uncertainties in  $m$  and  $b$  (equation 2; Table 2), correcting the magnitudes does not lead to a value of  $H_0$  with smaller errorbars. Indeed, as the errors in the corrected magnitudes are necessarily larger due to the uncertainties in  $m$  and  $b$ , this results in larger errors in  $\delta$  and in turn  $H_0$ .

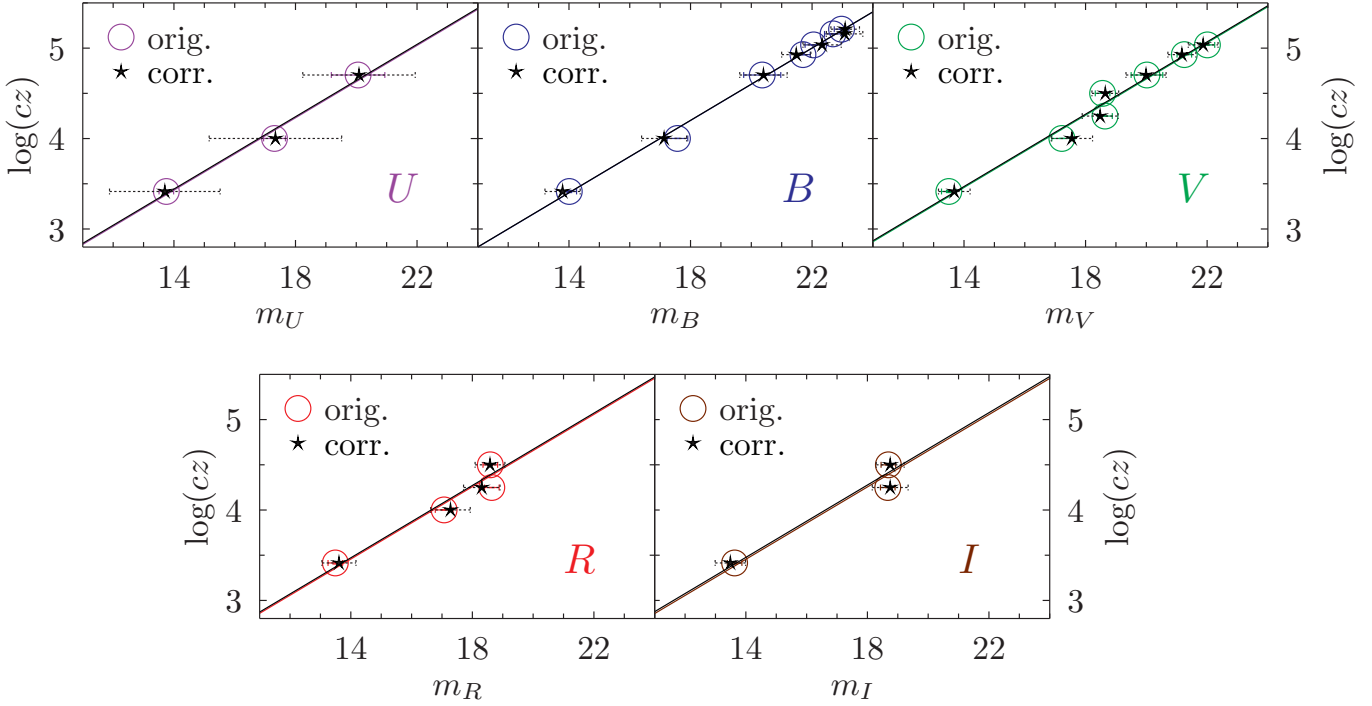


**Figure 3.** Hubble diagrams of the eight GRB-SNe from C14 in filters *UBVRI*. The solid line in each color is the best-fitting line to equation 3 to the uncorrected apparent peak magnitudes (open circles, solid-lined errorbars) in that filter, while the black, dotted line in each subplot is the fit to the corrected apparent peak magnitudes (black stars, dotted-lined errorbars). Note that there are errorbars in  $\log(cz)$ , however they are much smaller than the size of the datapoints.

Comparing the value of  $H_0$  among the five filters of original magnitudes, and for both statistical methods, gives a Hubble constant in the range of  $61\text{--}68 \text{ km s}^{-1} \text{ Mpc}^{-1}$ , with an average of  $H_0 = 64 \text{ km s}^{-1} \text{ Mpc}^{-1}$ . The standard deviation of the five filters is  $\sim 3 \text{ km s}^{-1} \text{ Mpc}^{-1}$ , which is of order the size of the error for each filter determined from the MC method, but is roughly 10 times smaller than the errors determined via the LLS method. This trend in relative error sizes is also seen when the corrected magnitudes (below) are used.

For the corrected magnitudes, a similar range of values is seen:  $63\text{--}69 \text{ km s}^{-1} \text{ Mpc}^{-1}$ , with an average value of  $H_0 = 66 \text{ km s}^{-1} \text{ Mpc}^{-1}$ . The standard deviation is again  $\sim 3 \text{ km s}^{-1} \text{ Mpc}^{-1}$ . In *B* and *V*, the error from the MC method is of order  $4\text{--}5 \text{ km s}^{-1} \text{ Mpc}^{-1}$ , but is larger in the other filters, with a max error of almost  $40 \text{ km s}^{-1} \text{ Mpc}^{-1}$  in the *U*-band. This large error can be attributed to the large errorbars of the corrected *U*-band magnitudes, which ultimately results from the errors of  $m$  and  $b$  in this filter.

Finally, using a different value of  $H_0$  to calculate the peak absolute magnitude of the GRB-SNe using cosmological models in Section 3.1 has a very small effect on the values of the Hubble constant derived here. For example, if we corrected our data using a luminosity–decline relationship that was obtained using  $H_0 = 80 \text{ km s}^{-1} \text{ Mpc}^{-1}$  (instead of  $67.3 \text{ km s}^{-1} \text{ Mpc}^{-1}$ ), we find a difference in the Hubble constant in the *U*-band of only  $\Delta H_0 = 0.05 \text{ km s}^{-1} \text{ Mpc}^{-1}$ , while the largest deviation is in the *B*-band, with  $\Delta H_0 = 0.53 \text{ km s}^{-1} \text{ Mpc}^{-1}$ . Therefore, the derived value of  $H_0$  obtained using GRB-SNe is insensitive (to within the errorbars determined via both fitting methods) to the values of the cosmological

parameters that are used to calibrate the luminosity–decline relationship in Section 3.1.

## 4 DISCUSSION & CONCLUSIONS

In this paper we demonstrated that GRB-SNe can, in principle, be used to determine one of the most fundamental cosmological parameters, the Hubble constant. We assumed the distance to SN 1998bw to be  $37 \text{ Mpc}$ , which is a good educated guess based on distances calculated using a redshift  $z = 0.00866$  and  $\Lambda\text{CDM}$  models with standard values, and using this, we constrained  $H_0$  to the range  $61\text{--}69 \text{ km s}^{-1} \text{ Mpc}^{-1}$ .

We used two statistical data-fitting procedures in our analysis, a LLS method and a MC method to first determine the luminosity–decline relationship for GRB-SNe (Fig. 2 and Table 2), and constrain the  $y$ -intercept ( $\delta$ ) of the Hubble line (equation 3) to ultimately determine  $H_0$ .

The errors in  $m$  and  $b$  in Section 3.1, and  $\delta$  and in  $H_0$  in Section 3.2, were determined via the two methods. In the LLS method, the errors are statistical, and determined by the fitting algorithm used by `PYXPLOT`. In the MC method, the  $1\text{-}\sigma$  errors are determined from the standard deviation of the distribution of values of each free parameter from 10,000 simulations. It was seen that the errors in  $m$  and  $b$  from the MC method were larger than the LLS method, while the errors in  $\delta$ , and thus  $H_0$ , were smaller in the MC method.

Currently, the propagated errors from  $m$  and  $b$  in equation 2, through to the peak apparent magnitudes that are fit with the Hubble line, result in larger errors in the Hubble constant than when the uncorrected magnitudes are used. It

may prove in the future however, with much larger datasets, that tighter luminosity–decline relations are obtained, thus reducing the scatter and errors in the fitted parameters, and ultimately reducing the error in  $H_0$ .

Interestingly, the weakest luminosity–decline correlation was seen in the  $B$ -band, however the same  $B$ -band data gives one of the tightest constraints (i.e. smallest errors) on the Hubble constant of all the filters. The  $V$ -band also provides a tight constrain on  $H_0$ , which like the  $B$ -band, may arise from the (relatively) larger datasets that span a wider range of distances/redshifts than the other filters ( $URI$ ).

We also investigated the what the effect would be if we used different values for the cosmological parameters to determine the distance moduli of the GRB-SNe (and their resultant peak absolute magnitudes) on the luminosity–decline relations, and the final derived value of the Hubble constant. In each case, the slope of the luminosity–decline relationship remained unchanged, while the  $y$ -intercept ( $b$ ) changed depending on the value of the Hubble constant that is used in the cosmology models to calculate the distance modulus. The propagated effect on the final value of  $H_0$  is minimal, with a difference of  $\Delta H_0 = 0.05\text{--}0.53 \text{ km s}^{-1} \text{ Mpc}^{-1}$ , with the largest deviation seen in the  $B$ -band. These differences are much smaller than the errorbars derived from the two fitting procedures.

Finally, in the long-run, GRB-SNe may prove to be even better cosmological probes than SNe Ia. From an evolutionary point of view, there are huge differences between GRB-SNe and SNe Ia. GRBs are a class of stellar explosions that are predominantly found in the high-redshift universe, and the production of a GRB-SN only requires a massive star, which can explode only a few million years after formation. Conversely, SNe Ia are formed by binary systems where at least one of the stars is a white dwarf, which takes billions of years to form. As such, GRB-SNe could in principle be found in the very early universe before a white dwarf has yet to form.

Fortunately, GRB-SNe peak at similar luminosities as SNe Ia, making them luminous enough to allow astronomers to use them as probes of the expansion of the universe beyond the redshift limits of SNe Ia. Moreover, with the hopeful launch of NASA’s James Webb Space Telescope in 2018, and the start of science observations in 2020, there remains a very real possibility to observe GRB-SNe to much higher redshifts than is currently possible, thus providing a larger distance range to constrain the matter and energy content of the universe.

## ACKNOWLEDGMENTS

We thank Gulli Björnsson for his insightful comments to the original manuscript. ZC and PJ gratefully acknowledge support from a Project Grant from the Icelandic Research Fund.

## REFERENCES

Bazin, G., Ruhlmann-Kleider, V., Palanque-Delabrouille, N., et al. 2011, *A&A*, 534, A43  
 Cano, Z., et al. 2011, *ApJ*, 740, 41C

Cano, Z. 2013, *MNRAS*, 434, 1098  
 Cano, Z., de Ugarte Postigo, A., Pozanenko, A., et al. 2014, *A&A*, 568, A19  
 Cano, Z. 2014 (C14), *ApJ* (accepted), arXiv:1407.2589  
 Cenko, S. B., Perley, D. A., Jankkarinen, V., Burbidge, M., Diego, U. S., & Miller, K. 2009, *GRB Coordinates Network*, 9518, 1  
 Cucchiara, A., & Perley, D. 2013, *GRB Coordinates Network*, 15144, 1  
 Galama, T. J., et al. 1998, *Nature*, 395, 670  
 Freedman, W. L., Madore, B. F., Gibson, B. K., et al. 2001, *ApJ*, 553, 47  
 Garnavich, P. M., Stanek, K. Z., Wyrzykowski, L., et al. 2003, *ApJ*, 582, 924  
 Gorosabel, J., Pérez-Ramírez, D., Sollerman, J., et al. 2005, *A&A*, 444, 711  
 Jones, D. O., Rodney, S. A., Riess, A. G., et al. 2013, *ApJ*, 768, 166  
 Kowal, C. T. 1968, *AJ*, 73, 1021  
 Li, X., & Hjorth, J. 2014, arXiv:1407.3506  
 Margutti, R., et al. 2007, *A&A*, 474, 815  
 Patat, F., et al. 2001, *ApJ*, 555, 900  
 Perlmutter, S., Gabi, S., Goldhaber, G., et al. 1997, *ApJ*, 483, 565  
 Perlmutter, S., Aldering, G., Goldhaber, G., et al. 1999, *ApJ*, 517, 565  
 Pian, E., et al. 2006, *Nature*, 442, 1011  
 Phillips, M. M. 1993, *ApJL*, 413, L105  
 Planck Collaboration, Ade, P. A. R., Aghanim, N., et al. 2013, arXiv:1303.5076  
 Riess, A. G., Filippenko, A. V., Challis, P., et al. 1998, *AJ*, 116, 1009  
 Sandage, A., & Tammann, G. A. 1993, *ApJ*, 415, 1  
 Schulze, S., Malesani, D., Cucchiara, A., et al. 2014, *A&A*, 566, A102  
 Starling, R. L. C., Wiersema, K., Levan, A. J., et al. 2011, *MNRAS*, 411, 2792  
 Tammann, G. A., Reindl, B., Thim, F., Saha, A., & Sandage, A. 2002, *A New Era in Cosmology*, 283, 258

This paper has been typeset from a  $\text{\TeX}$ / $\text{\LaTeX}$  file prepared by the author.

**Table 1.** Observational Properties of GRB-SNe

GRB	SN	$\log(cz)$	Ref.	Filter	$\Delta m_{15,\nu}$	$M_{\nu}^{\dagger}$
980425	1998bw	3.4146±0.0119	1	<i>U</i>	1.62±0.324	-19.16±0.24
-	-	-	-	<i>B</i>	1.18±0.236	-18.90±0.24
-	-	-	-	<i>V</i>	0.84±0.168	-19.41±0.24
-	-	-	-	<i>R</i>	0.63±0.126	-19.42±0.24
-	-	-	-	<i>I</i>	0.44±0.088	-19.28±0.24
011121	2001fe	5.0358±0.0012	2	<i>B</i>	1.33±0.27	-19.30±0.28
-	-	-	-	<i>V</i>	0.71±0.14	-19.34±0.24
030329	2003dh	4.7029±0.0005	3	<i>U</i>	1.30±0.26	-19.56±0.88
-	-	-	-	<i>B</i>	1.01±0.202	-19.26±0.61
-	-	-	-	<i>V</i>	0.63±0.14	-19.60±0.52
031203	2003lw	4.4998±0.0003	4	<i>V</i>	0.51±0.102	-19.96±0.24
-	-	-	-	<i>R</i>	0.44±0.088	-19.93±0.24
-	-	-	-	<i>I</i>	0.36±0.072	-19.83±0.24
060218	2006aj	4.0011±0.0003	5	<i>U</i>	2.23±0.46	-18.61±0.36
-	-	-	-	<i>B</i>	1.69±0.338	-18.35±0.34
-	-	-	-	<i>V</i>	1.28±0.36	-18.70±0.33
-	-	-	-	<i>R</i>	0.82±0.164	-18.85±0.29
090618	-	5.2095±0.0008*	6	<i>B</i>	0.66±0.13	-19.57±0.24
100316D	2010bh	4.2487±0.0007	7	<i>V</i>	1.10±0.22	-18.55±0.24
-	-	-	-	<i>R</i>	0.75±0.15	-18.55±0.24
-	-	-	-	<i>I</i>	0.66±0.132	-18.52±0.24
120422A	2012bz	4.9282±0.0001	8	<i>B</i>	0.71±0.142	-19.19±0.24
-	-	-	-	<i>V</i>	0.59±0.118	-19.64±0.24
130831A	2013fu	5.1575±0.0009*	9	<i>B</i>	1.19±0.238	-19.49±0.28

<sup>†</sup> Absolute magnitudes are observer-frame and rest-frame extinction corrected, and are calculated using a flat  $\Lambda$ CDM cosmology with  $H_0 = 67.3 \text{ km s}^{-1} \text{ Mpc}^{-1}$ ,  $\Omega_M = 0.315$ ,  $\Omega_{\Lambda} = 0.685$ .

\* No error in the redshift quoted in the literature, so an error of  $\Delta z = 0.001$  is assumed.

References: (1) Li & Hjorth (2014); (2) Garnavich et al. (2003); (3) Gorosabel et al. (2005); (4) Margutti et al. (2007); (5) Pian et al. (2006); (6) Cenko et al. (2009); (7) Starling et al. (2011); (8) Schulze et al. (2014); (9) Cucchiara & Perley (2013)

**Table 2.** Luminosity–decline relation: best-fitting parameters

Filter	LLS		MC		<i>r</i>	<i>p</i>
	<i>m</i>	<i>b</i>	<i>m</i>	<i>b</i>		
<i>U</i>	1.036±0.658	-20.886±1.190	1.039±0.816	-20.891±1.473	0.996	0.056
<i>B</i>	0.634±0.319	-19.863±0.353	0.584±0.239	-19.817±0.244	0.716	0.070
<i>V</i>	1.960±0.402	-20.872±0.335	1.739±0.421	-20.724±0.312	0.944	0.001
<i>R</i>	3.415±0.880	-21.442±0.582	3.238±0.994	-21.338±0.608	0.922	0.078
<i>I</i>	4.418±1.093	-21.360±0.550	4.404±1.595	-21.356±0.735	0.985	0.109

LLS = Linear Least Squares regression analysis.

MC = Monte-Carlo analysis.

*r* = Pearson’s correlation coefficient.

*p* = two-point probability of a chance correlation.

**Table 3.** Hubble Constant,  $H_0$  ( $\text{km s}^{-1} \text{ Mpc}^{-1}$ ), calculations

Filter	uncorr. LLS		uncorr. MC		corr. LLS		corr. MC	
	$\delta$	$H_0$	$\delta$	$H_0$	$\delta$	$H_0$	$\delta$	$H_0$
<i>U</i>	0.629±0.195	64.74±36.63	0.629±0.023	64.71±3.52	0.641±1.115	66.85±800.62	0.647±0.195	67.45±38.23
<i>B</i>	0.600±0.106	68.18±18.85	0.600±0.012	68.23±1.91	0.601±0.220	68.45±45.23	0.602±0.025	68.55±4.06
<i>V</i>	0.658±0.100	61.67±16.00	0.658±0.012	61.66±1.73	0.669±0.200	63.29±36.94	0.675±0.031	64.12±4.74
<i>R</i>	0.657±0.125	61.24±20.43	0.657±0.015	61.24±2.15	0.672±0.283	63.32±58.13	0.675±0.073	63.83±11.68
<i>I</i>	0.655±0.139	65.02±24.44	0.655±0.016	65.01±2.44	0.676±0.294	68.26±65.95	0.682±0.100	69.18±17.19
	$H_0 =$	64.17	$H_0 =$	64.17	$H_0 =$	65.98	$H_0 =$	66.63
	$\sigma =$	2.82	$\sigma =$	2.85	$\sigma =$	2.55	$\sigma =$	2.50

LLS = Linear Least Squares regression analysis.

MC = Monte-Carlo analysis.

$\delta$  = *y*-intercept of Hubble line (Fig. 3).